Sedimentary Geology 389 (2019) 91–102

Contents lists available at ScienceDirect

Sedimentary Geology

journal homepage: www.elsevier.com/locate/sedgeo

Optimizing subsampling strategies for U/Th dating and geochemical proxies in carbonate speleothems

Christine Perrin [a,*], Romain Tilhac [b], Laurent Prestimonaco [c]

[a] Département Homme et Environnement, Muséum National d'Histoire Naturelle, HNHP UMR7194 CNRS-MNHN-UPVD, Centre Européen de Recherche en Préhistoire, Avenue Léon-Jean Gregory, 66720 Tautavel, France
[b] ARC Centre of Excellence for Core to Crust Fluid Systems (CCFS) and GEMOC, Department of Earth and Planetary Sciences, Macquarie University, Sydney, NSW 2109, Australia
[c] Aquila Conseil, Parc Industriel de la Piche, Avenue Pierre Semard, 31600 Seysses, France

ARTICLE INFO

Article history:
Received 4 April 2019
Received in revised form 3 June 2019
Accepted 4 June 2019
Available online 10 June 2019

Editor: Dr. J. Knight

Keywords:
Speleothem
Diagenesis
Radiometric dating
XRF
Trace element
Aragonite

ABSTRACT

Since they provide the chronological frame on which paleoclimate and paleoenvironmental reconstructions are built, radiometric ages of carbonate speleothems, especially U/Th dating, are of fundamental importance to speleothem and paleoclimate sciences. Based on 17 aragonite-calcite speleothems from the Pont-de-Ratz Cave (S. France), we propose an integrated petrographical and geochemical approach for optimizing subsampling in speleothems. Portable energy-dispersive X-ray fluorescence was used as a fast and non-destructive in-situ trace-element screening of the speleothems. These geochemical results are combined with petrographical and mineralogical information to produce distribution maps showing the growth discontinuities and the identified primary and secondary (diagenetic) products on the speleothem slabs. Because they provide a clear and precise spatial distribution of primary and secondary carbonate phases at the sample scale, these maps constitute a valuable tool for selecting the position of subsamples for radiometric dating or environmental proxy analysis. The efficiency and reliability of our integrative approach is convincingly demonstrated by the remarkable coherence of U/Th ages both within and between speleothem samples.

1. Introduction

Radiometric dating of speleothems such as U/Th age-series dating, is crucial for the understanding of the growth history of individual speleothems and the related physico-chemical conditions, and thus for reconstructing past climates and environmental fluctuations from geochemical proxies. Obtaining reliable radiometric ages is particularly important because these provide the precise chronological framework in which the climatic and environmental scenarios can be integrated.

For this purpose, a fundamental pre-requisite is that spelean material has not undergone pervasive diagenesis since its deposit, and that its isotopic composition (including U and Th isotopes) has evolved under conservative closed or semi-closed chemical conditions. Diagenetic alteration may strongly impact both U/Th dating and the original environmental signal, notably in terms of stable isotopes (Frisia et al., 2002; Woo and Choi, 2006; Martin-Garcia et al., 2009; Zhang et al., 2014) and trace-element proxies such as Sr/Ca and Mg/Ca ratios (Perrin et al., 2014; Dominguez-Villar et al., 2017), leading to misleading and/or contradictory reconstructions of past climates and paleoenvironmental conditions.

Usually, in age-series, outliers and points yielding inversion-age are discarded. While the exclusion of these ages is usually discussed in relation with age-model construction (e.g., Columbu et al., 2017), the potential causes for these outliers are only rarely explored (Scholz et al., 2014; Bajo et al., 2016).

It has been however demonstrated from numerous speleothem materials sampled in caves worldwide that even subtle post-depositional alteration may induce re-mobilization of U, particularly during recrystallization of aragonite into calcite, and therefore yielding erroneous U/Th ages (e.g., Railsback et al., 2002; Hopley et al., 2009; Lachniet et al., 2012a; Bajo et al., 2016; Martin-Garcia et al., 2019). The impact of diagenesis on U/Th ages, stable isotope systematics and trace-element ratios has also been shown in biological aragonite material such as scleractinian corals (Ribaud-Laurenti et al., 2001; Li and Jones, 2013; Lazar et al., 2014). For these reasons, most speleothem-based paleoclimate reconstructions use calcite material while aragonite speleothems, which are more prone to diagenesis, tend to be avoided. However, aragonite speleothems are particularly well suited as climate and environmental recorders (e.g., Finch et al., 2001, 2003; Lachniet et al., 2012b; Lachniet, 2015) and offer much better dating precision than their calcite counterparts. Moreover, recent work has shown that in some diagenetically altered aragonite speleothem, the $\delta^{13}C$ values of secondary calcites are inherited from their aragonite precursor and can potentially be used in paleoclimate and paleoenvironmental

* Corresponding author.
E-mail address: cperrin@mnhn.fr (C. Perrin).

https://doi.org/10.1016/j.sedgeo.2019.06.002
0037-0738/

recronstructions (Zhang et al., 2014). There is hence a strong need for developing an approach to the screening of diagenetic effects in aragonite and potentially altered calcite speleothems.

Although corrections for detrital Th contamination do exist (e.g., Hellstrom, 2006) and rather sophisticated models for extrapolating points between measured radiometric ages are available (Scholz and Hoffmann, 2011; Hercman and Pawlak, 2012; Scholz et al., 2012), detailed petrographical analysis remains the most reliable and straightforward method for deciphering diagenetic features and thus the most suitable subsampling locations for such dating.

The aim of this paper is to describe and propose an integrated petrographical and geochemical approach for optimizing sampling strategies for radiometric dating and the analysis of environmental proxies in speleothems. Such optimization is notably required for study of either aragonite samples or calcite speleothems in which diagenesis is suspected. For that purpose, the case study of a well-characterized set of aragonite, aragonite-calcite, and calcite speleothems from the Pont-de-Ratz Cave (Saint-Pons-de-Thomières, S. France) is proposed. First investigations on speleothems of the Pont-de-Ratz Cave were conducted in the pioneering work of Cabrol (1978) and Cabrol and Coudray (1982). Detailed petrographical and geochemical studies of some Pont-de-Ratz samples were then reported in Perrin et al. (2013, 2014) which identified the growth and diagenetic history of the speleothems over the last 10,000 years. On the basis of this work, the present paper reports and discuss: (1) new and complementary data obtained from additional speleothems from the same site in the cave, in particular the use of portable X-ray fluorescence spectrometry, (2) the spatial distribution of primary and diagenetic products on speleothems slabs, (3) its use as a tool for selecting suitable subsamples for U/Th dating, and (4) U/Th ages.

2. Geographical and geological setting

The Pont-de-Ratz Cave is located on the southern margin of the Montagne Noire (Hérault, S. France) ~45 km NE of Carcassonne (Fig. 1). The cave bedrock consists of dolomites and limestones of Lower Devonian (Pragian to lower Emsian) age (Alabouvette et al., 1993). The cave itself is formed by three upper fossil levels and one active level where an underground stream currently flows. The speleothems used for this study were collected in the Cimetière Chamber, so called after an act of vandalism occurred in the 1970s destroying most of the stalactites and stalagmites in this room. The broken speleothems were left in place after the destruction. The material used for our research work was sampled among the already broken speleothems of this site.

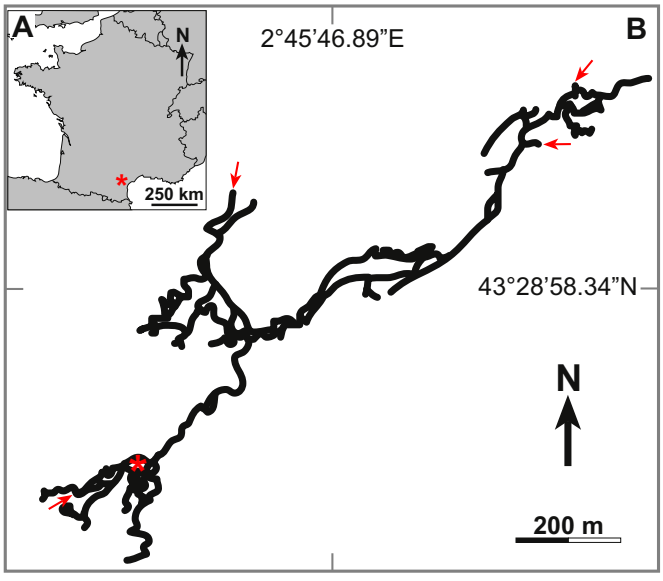

Fig. 1. (A) Geographical setting of the Pont-de-Ratz Cave in southern France; (B) general map of the cave, red arrows indicate the main cave entrances, red star shows location of the sample site. (For interpretation of the references to color in this figure legend, the reader is referred to the web version of this article.)

3. Material and methods

3.1. Methodological approach

The proposed methodological approach for optimizing subsampling of speleothems is based on a suite of analytical techniques aiming (1) to distinguish primary and secondary (diagenetic) features, (2) to precisely report the distribution of these identified features at the scale of individual speleothems, and finally (3) to use this information for selecting the best preserved spots (i.e., devoid of diagenesis) for subsampling.

Speleothem-based paleoclimate studies require numerous analyses to be performed on a limited amount of material, often restricted to the axial part of a stalagmite. That is why the proposed approach favors non-destructive analytical techniques such as portable energy-dispersive X-ray Fluorescence Spectrometry (P-XRF) and Raman microspectrometry over those that consume more carbonate material.

Following speleothem cutting (Fig. 2, step 1) and first observation under a binocular microscope on the polished surface slabs (Fig. 2, step 2), P-XRF analyses are performed on each slab surface (i.e., 4 to 6 surfaces per individual speleothem, depending on its size; Fig. 2, step 3). P-XRF is used as a rapid in-situ non-destructive first screening method, which requires no sample preparation except polishing and cleaning, and the size of the analytical spot (~1 cm-square, see below) is particularly well suited for an assessment at scale of the entire speleothem. Based on binocular observations and P-XRF results, locations of thin sections are then selected on one median slab (Fig. 2, step 4). Petrographical study of thin sections (Fig. 2, step 5) is based on optical microscopy and, when necessary, on Raman microspectrometry and/or other techniques such as scanning electronic microscopy and electronic microprobe (see Perrin et al., 2014, for the use of these two last techniques on the Pont-de-Ratz speleothems). The primary and secondary carbonate products and other petrographical features such as discontinuities are mapped on each thin section (Fig. 2, step 6). These petrographical maps are then used as a reliable guide to select the best (i.e., unaltered) areas for subsampling the symmetric slab for radiometric dating and environmental proxies.

3.2. Analytical techniques and material

In total, fourteen stalagmites, two stalactites and one flowstone (Fig. 3; Table 1) were cut parallel to their general median growth axis with a diamond saw in order to get two slabs on either side of their vertical median plan or one median slab in small size speleothems. Each slab was polished, ultrasonic-cleaned, scanned and observed under the binocular microscope.

A subset of trace elements (Mn, Fe, Zn, Sr, and Zr) was measured in-situ on each slab surfaces using an Innov-X portable energy-dispersive X-ray fluorescence spectrometer. Analyses were run at 10–30 Kv for a duration of ~50–60 s per analytical point (N = 182 for the whole data set). Before each analytical session, the P-XRF spectrometer was calibrated with a standard Alloy 316 Stainless Steel target provided by the manufacturer. Quantification of elementary concentrations is performed internally by the spectrometer using the Compton Normalization calibration which has been proved to provide robust calibration and minimize matrix effects. The spatial resolution of the Innov-X P-XRF spectrometer is ~1 cm-square for a sampling depth of a few micrometers. This technique does not allow the analysis of lighter elements such as Mg, Si or Al. However, the detection limit for most trace elements commonly occurring in carbonate speleothems is similar or

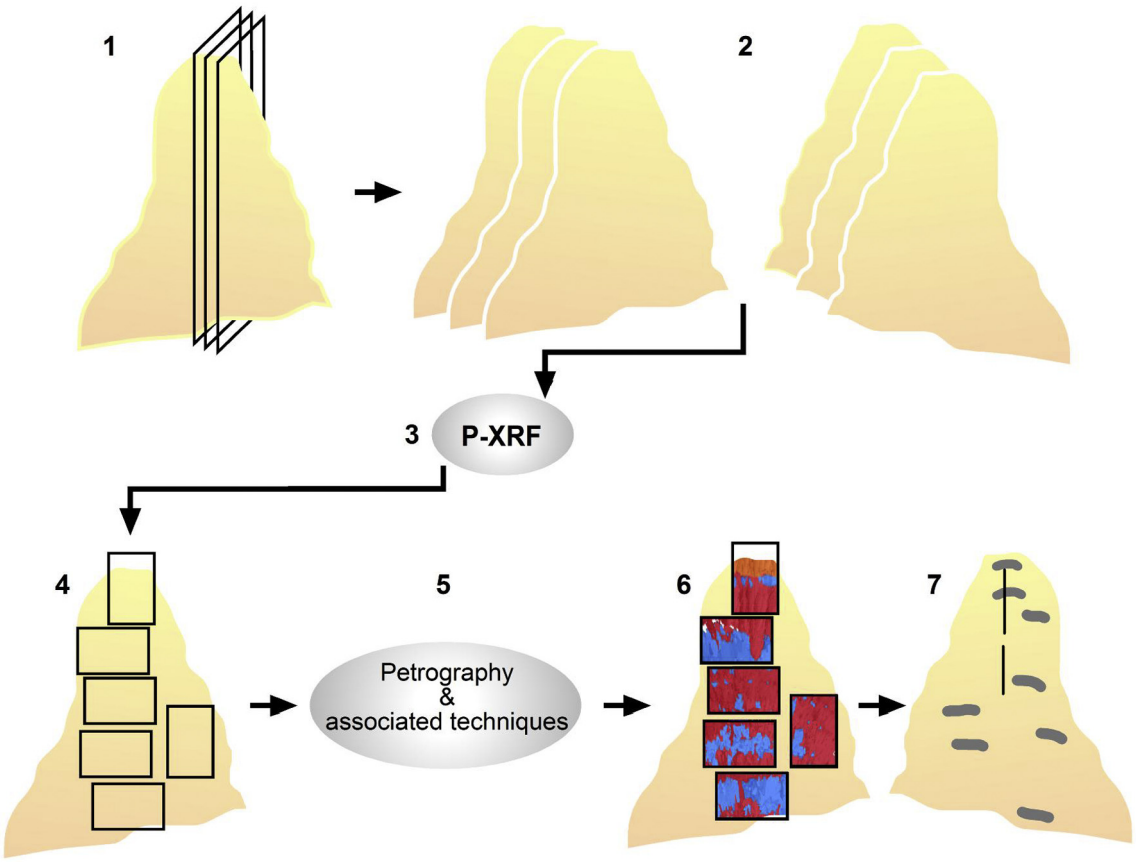

Fig. 2. Main successive steps of the integrated approach used in the present work. Cutting the speleothem parallel to their median growth axis (1) provides one or two slices (depending on the sample size) and 4 to 6 slab surfaces. (2) P-XRF spectrometry is performed on each slab surfaces. (3) On the basis of these P-XRF results and binocular observations, locations are selected in a slab for thin-sectioning. (4) Petrographical study of thin sections is based on optical microscopy and Raman microspectrometry, eventually associated with SEM and electronic microprobe. (5) The different petrographical features are then mapped on each thin section. (6) These petrographical maps are then used for optimizing subsampling of the symmetric slab for U—Th dating and paleoclimate proxies.

significantly lower than the one obtained with a wavelength-dispersive X-ray spectrometry electron microprobe. In our Pont-de-Ratz samples, the limits of detection are the following: 180 ppm (Mn), 180 ppm (Fe), 30 ppm (Zn), 4 ppm (Sr), and 30 ppm (Zr). Considering the low limit of detection of these elements and the shallow sampling depth of the P-XRF analyses, particular attention was thus paid to operate on clean sample surfaces.

One median slab per speleothem was prepared for petrographical observations. 41 large (6 × 4 cm) and 10 standard (2 × 3 cm) thin sections, 20–25 μm in thickness were prepared, mostly cut parallel to the general growth direction of the speleothem and observed with conventional petrographical microscopes.

Raman microspectrometry was used for complementary mineralogical identifications of carbonate species, in particular when determination of mineralogy was difficult or uncertain from optical microscopy only. Analyses were conducted on selected polished samples and thin sections with a Jobin Yvon Horiba HR800 LabRamH spectrometer operating with a green 514.5 nm exciting line using ~10 mW on sample, and with a 1 mm spatial pseudo-confocal filter to reduce analysis at depth. The Raman spectrometer is equipped with a reflected light optical microscope and a video camera which allow the laser spot to be precisely and visually positioned. Analyses were run with a spectral window of 130–1600 cm^{-1} and a spatial resolution of ~1–2 μm. Potential deviation of the Raman spectrometer was corrected if needed by measuring the spectrum of a known quartz crystal before each analytical session.

Five stalagmites (PDR3, PDR17, PDR20, PDR21, PDR22) were sampled for U/Th dating using a micro-diamond saw. U/Th dating was performed in two batches by thermal-ionization mass spectrometry (TIMS) on a Triton Plus and multi-collector inductively coupled plasma mass spectrometry (MC-ICP-MS), respectively, at the Geotop (Montreal, Canada). Fourteen U/Th ages were obtained from either aragonite or calcite subsamples, including 8 from TIMS (average weight 3.3 g for aragonite subsamples and 8.7 g for calcite subsamples) and 6 from MC-ICP-MS (average weight 0.9 g for aragonite subsamples and 3.9 g for calcite subsamples), following the analytical procedure used at the Geotop (Genty et al., 2010; Gázquez et al., 2014; Pozzi et al., 2019).

4. Summary of previous work: primary and diagenetic features in the Pont-de-Ratz speleothems

Perrin et al. (2014) have shown that the growth of Pont-de-Ratz speleothems alternatively occurred through the precipitation of two distinct primary aragonites: (1) primary acicular and ray aragonite, (2) primary bladed aragonite, and a primary columnar calcite (Table 2). Four types of growth discontinuities and inclusion horizon: (1) growth surface related to one or several inclusion levels, (2) growth surface marked by a detrital layer, (3) growth discontinuity resulting from change of crystallization, (4) growth discontinuity associated with dissolution have also been identified, suggesting that the speleothem growth was periodically interrupted (see Perrin et al., 2014, their Table 4 p. 263).

Spelean primary precipitates are affected by post-depositional diagenetic processes taking place at, or more commonly, below the outer surface of speleothem, namely cementation, dissolution, and recrystallization of extant primary minerals (Table 2).

Two distinct calcite cements (as sparry crystals and small isolated rhombohedrons, respectively), precipitated where inter-crystalline porosity and permeability were sufficient for the drip water to infiltrate

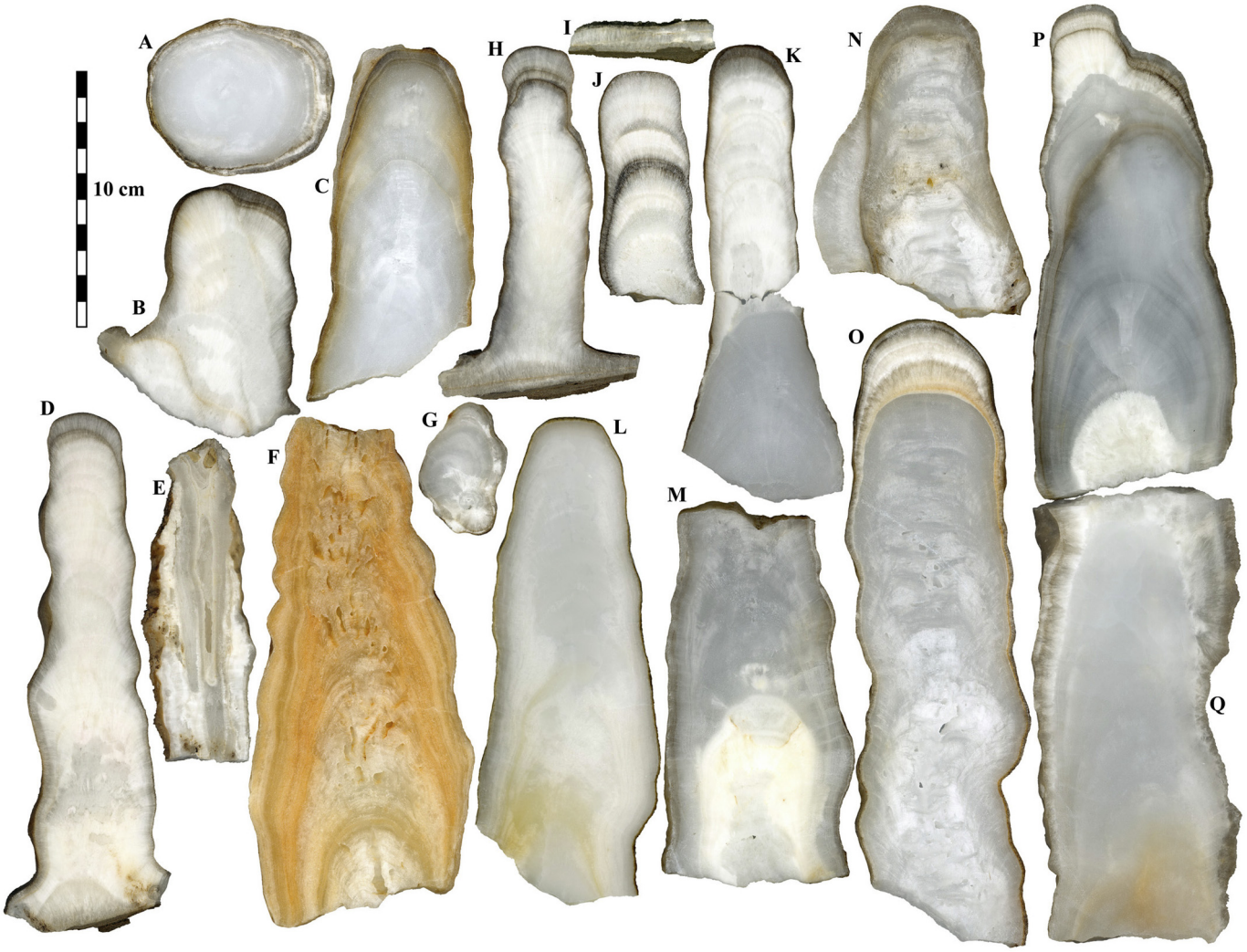

Fig. 3. The speleothems of the Pont-de-Ratz cave used for this study. (A) Slab of stalagmite PDR7. (B) Slab of stalagmite PDR5. (C) Slab of stalagmite PDR6. (D) Slab of stalagmite PDR12. (E) Slab of stalagmite PDR18. (F) Slab of stalagmite PDR22. (G) Slab of stalagmite PDR8. (H) Slab of stalagmite PDR17. (I) Slab of stalagmite PDR15. (J) Slab of stalagmite PDR2. (K) Slab of stalagmite PDR21. (L) Slab of stalagmite PDR25. (M) Slab of stalagmite PDR1. (N) Slab of stalagmite PDR3. (O) Slab of stalagmite PDR20. (P) Slab of stalagmite PDR19B. (Q) Slab of stalagmite PDR19A.

below the outer surface of the speleothem. Precipitation of the small isolated rhomboedral crystals has been interpreted as the first step of recrystallization of primary aragonite into columnar calcite (Perrin et al. 2014, their Fig. 15 p. 262). Three types of recrystallization have been identified in the Pont-de-Ratz speleothems: aragonite to aragonite recrystallization which mainly occurs through textural change,

Table 1
Description of the speleothems used for this study. All samples are from the Cimetière chamber of the Pont-de-Ratz cave. Note that unit numbers are not correlated across samples. AR1, primary aragonite; AR2, secondary aragonite; CC1, primary columnar calcite; CC2, secondary columnar calcite; CS2, secondary sparry calcite.

Sample	Speleothem type	Length (mm)	Short description
PDR1	Stalagmite	148	Basal unit: acicular AR1 partly recrystallized to AR2, CS2, CC2. Unit 2: CC1. Unit 3: bladed AR1.
PDR2	Stalagmite	92	Acicular and ray AR1 in 4 main growth units, aragonite recrystallized in a few places to CC2.
PDR3	Stalagmite	122	2 basal units in columnar calcite. Unit 3: bladed AR1 partly recrystallized to CC2. Unit 4: CC1.
PDR5	Stalagmite	99	Acicular and ray AR1 in 4 main growth units, aragonite recrystallized in a few places to CS2 and CC2.
PDR6	Stalagmite	~137	Columnar calcite stalagmite in main growth units.
PDR7	Stalagmite	NA	Transverse section of stalagmite: columnar calcite in the central part, acicular and ray AR1 in external parts.
PDR8	Stalactite	NA	Ray and acicular AR1, partly recrystallized to CC2.
PDR12	Stalagmite	201; 70	Two stalagmites on basal flowstone. Ray and acicular AR1 in 3 main growth units, AR1 partly recrystallized to CS2.
PDR15	Flowstone	NA	Basal flowstone. Ray AR1 on fluvial sand.
PDR17	Stalagmite	133	Ray and acicular AR1.
PDR18	Stalactite	126	Ray and acicular AR1 partly recrystallized to CS2.
PDR19A	Stalagmite	177	Basal unit: CC1. Unit 2: acicular AR1 partly recrystallized to CS2.
PDR19B	Stalagmite	193	Acicular AR1 partly recrystallized to CS2 and CC2. Unit 3: CC1. Unit 4: AR1 mostly recrystallized to CC2. Unit 5: CC1. Units 6–8: acicular and ray AR1.
PDR20	Stalagmite	252	Basal unit: CC1. Unit 2–5: ray and acicular AR1.
PDR21	Stalagmite	180	Basal unit: CC1. Unit 2: acicular AR1 partly recrystallized to CS2 and to CC2. Units 3 and 4: ray AR1.
PDR22	Stalagmite	200	Fe-rich stalagmite entirely formed of CC1.
PDR25	Stalagmite	191	CC1 followed by ray aragonite.

Table 2
Main primary and diagenetic carbonate products characterized by Perrin et al. (2014) in speleothems of the Pont-de-Ratz cave.

	Carbonate products	Petrography	Remark on diagenetic process
Speleothem growth	Primary aragonite	Acicular and ray aragonite	/
		Bladed aragonite	/
	Primary calcite	Columnar calcite	/
Speleothem diagenesis	Calcite cement	Sparry calcite	Precipitation in voids of pre-existing structure (primary porosity)
		Isolated rhombohedral crystals	Precipitation in intercrystalline porosity of primary aragonite. 1st step of recrystallization ray aragonite – columnar calcite
	Secondary aragonite	Ray aragonite	Recrystallization aragonite - aragonite
	Secondary calcite	Sparry calcite	Recrystallization aragonite - calcite: recharge rate of diagenetic fluid slow with respect to kinetics of recrystallization
	Secondary calcite	Columnar calcite	Recrystallization aragonite - calcite: recharge rate of diagenetic fluid high with respect to kinetics of recrystallization

aragonite to sparry calcite recrystallization, and aragonite to columnar calcite recrystallization (Table 2). Both types of aragonite to calcite recrystallization impact the initial geochemical signature of the speleothem but they affect the Mg/Ca and Sr/Ca ratios differently (see Perrin et al. 2014, their Table 5 p. 266 for detail) as a result from differences in the balance between the recharge rate of diagenetic fluid and the kinetics of recrystallization (Table 2).

5. Results

5.1. P-XRF results

Sr is the most common element measured in our material, being detected in all analyses (Supplementary data file). The Sr content, since it can be measured with a limit of detection of a few ppm, is particularly

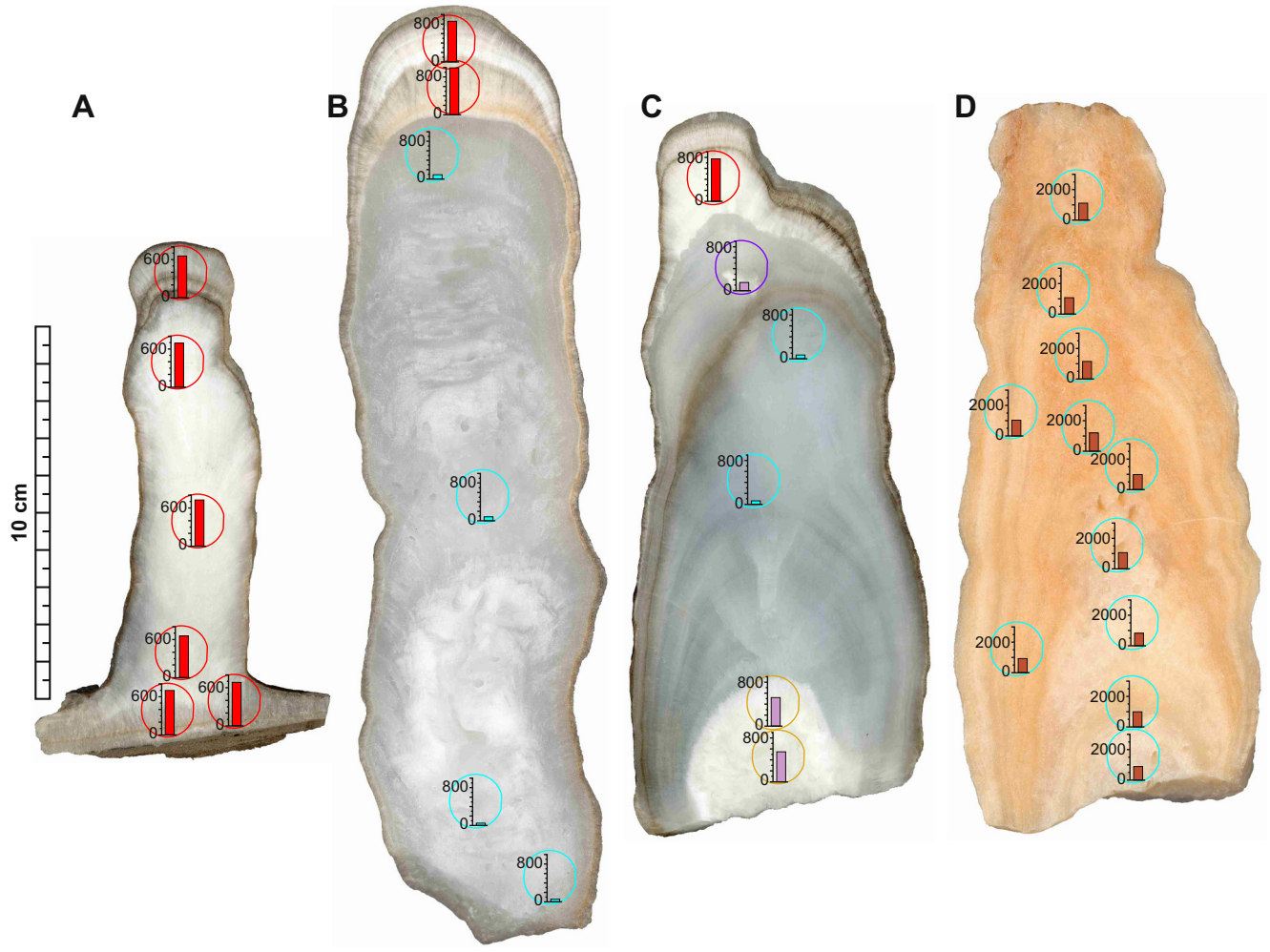

Fig. 4. Concentrations of strontium and iron from P-XRF spectrometry and their spatial distribution on stalagmite slabs. Plots show respective elemental concentrations of Sr for slabs A–C, and Fe for slab D, in ppm. Circles represent analytical spots of the P-XRF spectrometer. Red circles, primary aragonite; blue circles, primary columnar calcite; orange circles, recrystallization sparry calcite with abundant relics of primary aragonite; purple circle, analytical spot covering primary aragonite and secondary columnar calcite. Red plots are typical Sr values of primary aragonite; blue plots, typical Sr values of calcite. Purple plots show intermediate values between pure-aragonite and pure-calcite values. Orange plots on slab D correspond to Fe concentrations. (A) Slab of stalagmite PDR17. (B) Slab of stalagmite PDR20. (C) Slab of stalagmite PDR19B. (D) Slab of stalagmite PDR22. (For interpretation of the references to color in this figure legend, the reader is referred to the web version of this article.)

reliable. In the six largest samples of stalagmites investigated, the Sr content is not correlated with time (i.e., with stratigraphical position) neither in the primary aragonite (Figs. 4, 5) nor in the primary columnar calcite (not shown). This is also true (Figs. 4A, 5B) if three types of primary aragonite representing different growth stages are considered (i.e., the large ray-crystal aragonite forming the basal flowstone, the acicular aragonite, and the brown-gray aragonite making the uppermost part of some stalagmites, Fig. 3). Considering the spatial resolution of the technique, no variation or trend through time is detected within individual stalagmite samples. We consider therefore that the comparison of measurements by products on the whole set of samples and the use of averages are reasonable and meaningful (Table 3).

Sr is detected in both aragonite and calcite and displays contrasting proportions in the two carbonate polymorphs (Table 3, Supplementary data file). Sr content varies between ~650 and 998 ppm (on average 741 ± 85 ppm; 1σ) in primary aragonite, while it is restricted to 53–86 ppm and 55–74 ppm in primary and secondary (recrystallization) columnar calcite, respectively (Table 3, Fig. 4A–C). Such overlap between the Sr contents of both columnar calcites is observed independently from the speleothem sample, regardless of stratigraphical position within individual speleothem (Fig. 5A).

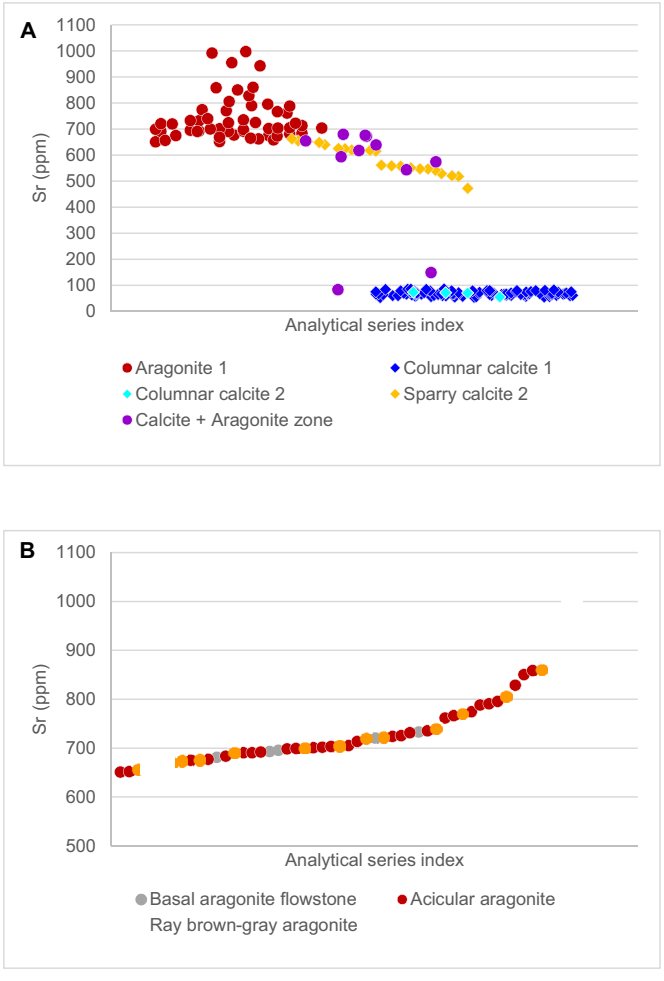

Fig. 5. (A) Strontium content of the primary and secondary carbonate phases of the Pont-de-Ratz speleothems from 179 P-XRF spectrometry analyses (including 108 previously used in Perrin et al., 2014, their Fig. 16). Aragonite 1, primary aragonite; Sparry calcite 2, secondary (recrystallization) sparry calcite; Columnar calcite 1, primary columnar calcite; Columnar calcite 2, secondary (recrystallization) columnar calcite; Calcite + Aragonite zone, analytical spot area including primary aragonite and columnar calcite. (B) Strontium content of three different types of primary aragonite. Total number of analyses: 53.

Analyses performed in areas consisting of secondary sparry calcite (i.e., resulting from recrystallization of primary aragonite to sparry calcite, Table 2), yielded rather high values of Sr ranging between 473 and 663 ppm (on average 585 ± 55 ppm; 1σ; Table 3, Fig. 4C). These values are slightly lower than those measured in primary aragonite (i.e., range 651–998 ppm, on average 741 ± 85 ppm; 1σ; Table 3) but markedly higher than those measured in primary and secondary columnar calcites (i.e., ranges 53–86 ppm and 55–71 ppm, on average 69 ± 9 ppm; 1σ and 68 ± 9 ppm; 1σ; Table 3; Fig. 4C). Measurements in areas covering both aragonite and calcite provided the widest range of Sr values (84–680 ppm) and the highest standard deviation (152 ppm, Table 3, Figs. 4C, 5A). The corresponding mean value (535 ppm) is identical within error to that obtained for recrystallization sparry calcite (585 ppm). In other words, recrystallized sparry calcite areas behave as a mixture of aragonite and calcite with respect to strontium (Fig. 5A).

When above detection limits, Mn and Fe can reach significant values in some analyses (up to 1007 and 383 ppm, respectively, Table 3), although Mn was detected sporadically (in less than 20% of analyses, Supplementary data file). The stalagmite PDR22, whose orange-color is characteristic of relatively high amounts of detrital material, yielded high contents of Fe consistently above the detection limit (Fig. 4D, Supplementary data file). Zn and Zr have been detected in some analyses of primary aragonite and primary columnar calcite but their concentrations remain close to the limit of detection and therefore have not been taken into consideration (Table 3, Supplementary data file).

5.2. Mapping original precipitates, growth discontinuities, and diagenetic products

The different petrographical features (i.e., growth discontinuities, primary and secondary carbonates) such as characterized in our previous study of the Pont-de-Ratz Cave (Perrin et al., 2014) have been mapped on the basis of petrographical observations and mineralogical identifications (from optical microscopy and Raman microspectrometry). Raman spectra record either aragonite, calcite or both minerals associated. The ν_4 symmetric CO_3 deformation band and both ν_3 asymmetric CO_3 stretching bands in the 1434–1574 cm^{-1} spectral region were used for discriminating both polymorphs (see Perrin and Smith, 2007a, 2007b, and Perrin et al., 2014, for detail on Raman vibrational bands in aragonite and calcite). A description of the growth units recognized in each speleothem used for the present work is reported in Table 1. These petrographical maps (Fig. 6) revealed quite useful when selecting suitable areas in these speleothems for subsampling spelean material for U/Th dating.

An example of such map is shown on Fig. 6. The first part of this stalagmite (PDR21) is composed by primary columnar calcite. Growth of this first phase of precipitation then stopped. This growth interruption is shown by discontinuity 1 (Fig. 7A). When carbonate precipitation resumed, acicular aragonite formed, suggesting changes in the local physico-chemical conditions. Subsequent growth interruptions (discontinuities 2 and 3) are observed close to the top of the stalagmite, marked by thin, inclusion-rich levels and a slight dissolution of the underlying ray-crystal aragonite (Fig. 7B).

In addition, the primary acicular aragonite has recrystallized into sparry calcite in some part of the stalagmite (Fig. 7C). The distribution of this secondary sparry calcite is not uniform at the sample scale, forming a core at the base of the primary acicular aragonite level above discontinuity 1. From this point upward, areas of secondary sparry calcite are organized in bands broadly parallel to the growth lamination of the stalagmite and alternating with levels of non- recrystallized primary acicular aragonite. This pattern which is the result of diagenesis, roughly reproduces the appearance of growth bands (Figs. 7C–D, 5D). The last carbonate precipitate at the top of the stalagmite consists of large brown-to-gray ray aragonite crystals (Fig. 6).

Table 3
Synthetic results of P-XRF spectrometry analyses of primary and secondary carbonate phases in speleothems of the Pont-de-Ratz Cave. N: number of analyses, LOD: limit of detection (see text for respective elemental values of LOD).

Nature	N		Mn	Fe	Zn	Sr	Zr
Primary aragonite	53	Range (ppm)	Up to 1007	Up to 383	<LOD	651–998	Up to 57
		Mean value (ppm)	112	100		741	Not significant
		Standard deviation (ppm)	187	127		85	
Primary columnar calcite	90	Range (ppm)	Up to 452	Up to 3162	Up to 34	53–86	Up to 50
		Mean value (ppm)	36	511	Not significant	69	Not significant
		Standard deviation (ppm)	102	508		9	
Secondary columnar calcite	4	Range (ppm)	<LOD	Up to 301	<LOD	55–74	<LOD
		Mean value (ppm)		148		68	
		Standard deviation (ppm)		130		9	
Recrystallization sparry calcite	21	Range (ppm)	Up to 332	Up to 835	<LOD	473–663	<LOD
		Mean value (ppm)	49	133		585	
		Standard deviation (ppm)	107	190		55	
Aragonite + calcite	11	Range (ppm)	<LOD	Up to 398	<LOD	84–680	<LOD
		Mean value (ppm)		102		535	
		Standard deviation (ppm)		151		152	

5.3. Selection of subsamples for U/Th dating

On the basis of the above petrographic considerations, subsamples for U/Th analyses were taken from zones entirely consisting of primary precipitates, either primary columnar calcite or primary aragonite, and avoiding recrystallized material (i.e., secondary sparry calcite and secondary columnar calcite) and areas affected by diagenesis (e.g., bearing secondary calcite cements; Fig. 6D).

5.4. U/Th results

5.4.1. U geochemistry and ^{232}Th content

U concentrations range from 0.07 to 6.59 ppm (Table 4) and show a marked difference between aragonite (5.27–6.59 ppm, mean value 5.99 ppm) and columnar calcite (0.07–0.18 ppm, mean value 0.13 ppm; Fig. 8A). These concentration ranges are comparable to those typically observed in continental carbonates including

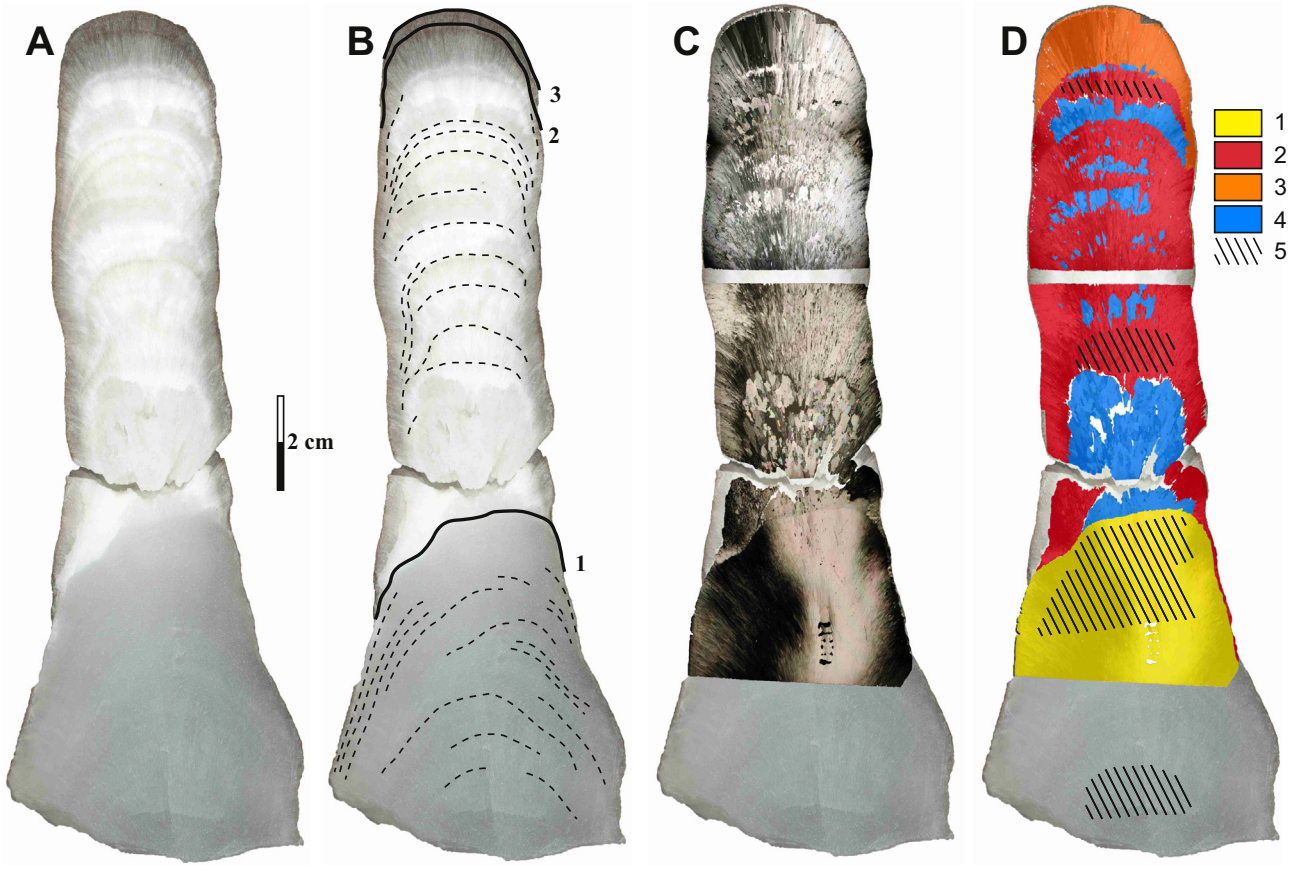

Fig. 6. Petrographical mapping of a stalagmite slab. (A) Polished slab of PDR21 stalagmite. (B) Same slab with the position of the three main discontinuity surfaces (solid lines). Some lamination are indicated by the thin dashed lines. (C) Position of the thin sections on the stalagmite slab. Thin sections are shown in polarized light with crossed-nichols. (D) Petrographical map showing the distribution of the primary and secondary carbonate phases at the scale of the stalagmite sample. 1, primary columnar calcite; 2, primary acicular aragonite; 3, primary ray aragonite; 4, recrystallization sparry calcite; 5, areas corresponding to subsampling for U/Th dating on the symmetric slab.

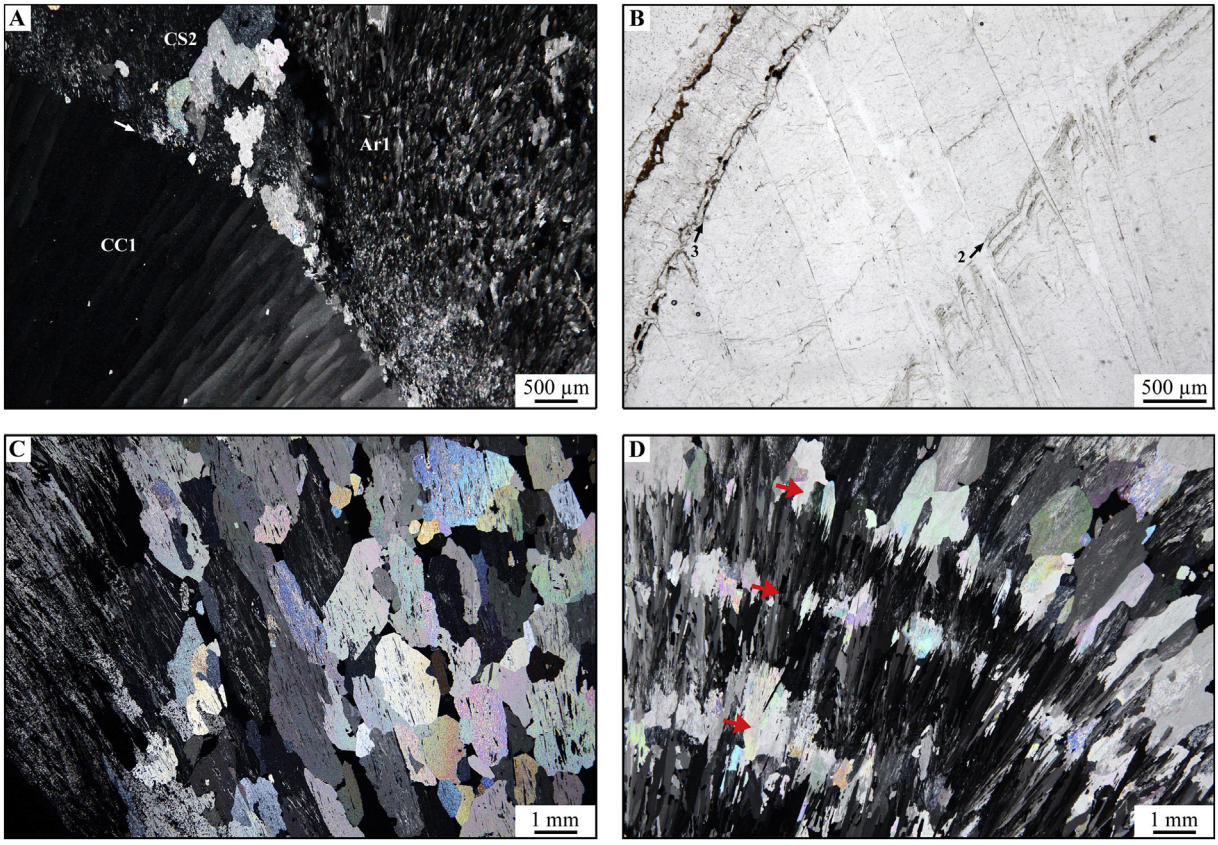

Fig. 7. Typical petrographical features observed in stalagmite PDR21 (see also Fig. 6), microphotographs of thin sections. (A) Growth discontinuity 1 (white arrow) occurring on top of primary columnar calcite (CC1) and followed by precipitation of primary acicular aragonite (Ar1). This primary aragonite was later recrystallized into sparry calcite (CS2), visible on the upper left side of the photograph; polarized light, crossed-nichols. (B) Growth discontinuities 2 and 3 (black arrows) in primary ray aragonite. Both discontinuities are marked by one or several inclusion levels and are associated with selective dissolution; polarized light. (C) Recrystallization of primary acicular aragonite into sparry calcite. Abundant relict crystals of aragonite are included in large sparry calcite crystals. Primary acicular aragonite affected by micro-dissolution is visible on the left part of the microphotograph; polarized light, crossed-nichols. (D) Recrystallization of primary acicular aragonite into sparry calcite preferentially follows some levels broadly parallel to growth lamination (red arrows), and forms alternating aragonite-calcite pseudo-growth bands; polarized light, crossed-nichols. (For interpretation of the references to color in this figure legend, the reader is referred to the web version of this article.)

speleothems, and much narrower than those found in diagenetically altered (i.e., recrystallized) speleothems (Railsback et al., 2002). The concentration of ^{238}U is not correlated with respect to the major growth phases (i.e., stratigraphical position) within each individual stalagmite (Fig. 8B).

Because the ^{232}Th is not part of the disintegration series of ^{238}U, it is generally used as an indicator of potential detrital contamination of the carbonate material with ^{230}Th, susceptible to alter the reliability of U—Th age. Our samples do not show any marked disparity between aragonite and calcite according to their ^{232}Th content. The Pont-de-Ratz primary aragonites have a ^{232}Th content varying between 0.03 and 1.77 ppb, and 0.03–0.22 ppb without the maximum value of 1.77 ppb measured in the ray brown-gray aragonite forming the top of stalagmite PDR17 (Table 4). The ^{232}Th concentrations in primary columnar calcites show a much wider range 0.02–4.53 ppb; the two higher values from the Fe-rich stalagmite PDR22, respectively reach 1.74 and 4.53 ppb.

5.4.2. U/Th ages

U/Th dating revealed that the speleothems sampled in the Cimetière Chamber of the Pont-de-Ratz Cave developed during the Holocene

Table 4
Uranium and thorium isotopic composition and calculated ages for subsamples of stalagmites from the Pont-de-Ratz Cave.

Sample	Mineralogy	^{238}U (ppm)	^{232}Th (ppb)	$^{234}U/^{238}U$	$^{230}Th/^{234}U$	$^{230}Th/^{238}U$	Calculated age (ky)
17-Uc	Aragonite	5.9999 ± 0.0240	1.7751 ± 0.0011	1.5739 ± 0.0044	0.0189 ± 0.0002	0.0297 ± 0.0003	2.0686 ± 0.0210
17-Ua	Aragonite	6.5841 ± 0.0321	0.0664 ± 0.0003	1.6477 ± 0.0099	0.0392 ± 0.0003	0.0646 ± 0.0005	4.3560 ± 0.0340
17-Ud	Aragonite	5.3304 ± 0.0263	0.0912 ± 0.0005	1.6357 ± 0.0035	0.0503 ± 0.0004	0.0823 ± 0.0007	5.5996 ± 0.0501
17-Ub	Aragonite	6.1447 ± 0.0254	0.2213 ± 0.0039	1.6475 ± 0.0064	0.0516 ± 0.0020	0.0850 ± 0.0033	5.7387 ± 0.2260
20-Ub	Calcite	0.1408 ± 0.0005	0.0205 ± 0.0001	1.8834 ± 0.0152	0.0670 ± 0.0010	0.1262 ± 0.0016	7.5340 ± 0.1160
20-Ua	Calcite	0.1688 ± 0.0007	0.0178 ± 0.0003	1.9337 ± 0.0172	0.0719 ± 0.0014	0.1390 ± 0.0025	8.1020 ± 0.1630
20-Uc	Calcite	0.1424 ± 0.0001	0.1330 ± 0.0001	1.9372 ± 0.0087	0.0719 ± 0.0014	0.1390 ± 0.0025	8.8480 ± 0.0810
21-Ud	Aragonite	6.5880 ± 0.0479	0.1925 ± 0.0012	1.7568 ± 0.0124	0.0348 ± 0.0004	0.0611 ± 0.0008	3.8380 ± 0.0583
21-Ub	Aragonite	5.2653 ± 0.0247	0.0349 ± 0.0002	1.8149 ± 0.0110	0.0628 ± 0.0005	0.1139 ± 0.0007	7.0500 ± 0.0580
21-Ua	Calcite	0.1215 ± 0.0005	0.0450 ± 0.0003	1.8173 ± 0.0218	0.0731 ± 0.0012	0.1328 ± 0.0016	8.2440 ± 0.1410
21-Ue	Calcite	0.0825 ± 0.0004	0.0324 ± 0.0003	1.9490 ± 0.0083	0.0959 ± 0.0011	0.1868 ± 0.0021	10.8739 ± 0.1387
22-Ub	Calcite	0.1739 ± 0.0006	4.5265 ± 0.0172	1.5857 ± 0.0132	0.0554 ± 0.0013	0.0878 ± 0.0020	6.2030 ± 0.1500
22-Ua	Calcite	0.1830 ± 0.0008	1.7356 ± 0.0078	1.6650 ± 0.0101	0.0543 ± 0.0001	0.0904 ± 0.0014	6.0750 ± 0.1030
3-Ua	Calcite	0.0780 ± 0.0003	0.0536 ± 0.0004	1.7011 ± 0.0103	0.0051 ± 0.0011	0.0086 ± 0.0019	0.5580 ± 0.1210

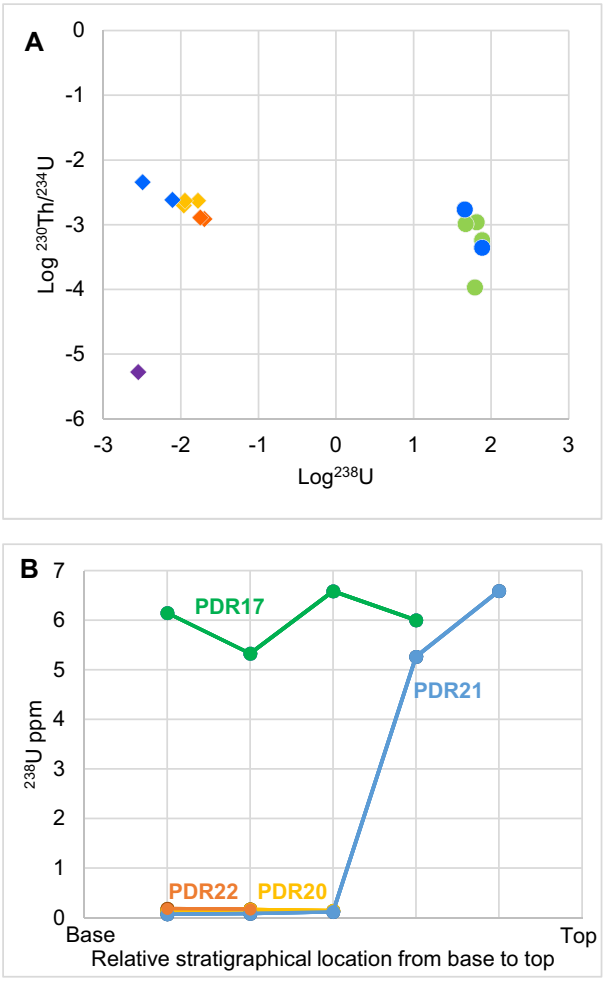

Fig. 8. (A) Log-log plot of ^{238}U concentration and $^{230}Th/^{234}U$ ratios of the subsamples from five stalagmites of Pont-de-Ratz Cave. Diamonds are calcite subsamples and dots represent aragonite subsamples. Each color correspond to one single stalagmite. Purple, PDR3 stalagmite; green, PDR17; yellow, PDR20; blue, PDR21; orange, PDR22. Aragonite and calcite subsamples show marked difference in U concentration although for the same mineralogy the U-concentration range remains rather narrow. (B) Variation of ^{238}U concentration with stratigraphical location of subsample in each individual stalagmite. Colors have the same significance as in (A). (For interpretation of the references to color in this figure legend, the reader is referred to the web version of this article.)

(Table 4), with ages ranging between 558 ± 121 yrs. and 10,874 ± 139 yrs. before present (BP). The distribution of these U/Th ages is remarkably consistent both within and across speleothem samples (Fig. 9). The sole apparent age-inversion occurs in the orange-colored stalagmite (Fig. 9C) and corresponds to the two primary columnar calcite subsamples having the highest ^{232}Th content mentioned above. Note however, that the age errors of these two U/Th ages overlap, likely as a consequence of the rather high growth rate of this stalagmite.

Our U/Th results also demonstrate that speleothems in this cave chamber developed in successive alternating periods of aragonite or calcite precipitation.

6. Discussion

6.1. Trace elements

6.1.1. Strontium as a tool for discriminating carbonate mineralogy

Strontium is detected in both aragonite and calcite but there are strong differences in its concentration, aragonite having about twelve times more strontium than columnar calcite. In the Pont-de-Ratz speleothems, Sr has been demonstrated to be hosted in the carbonate lattice (Perrin et al., 2014), where it substitutes for Ca^{2+} (Finch and Allison, 2007). Trace-element concentration in minerals is crystallographically constrained: the substitution of Ca^{2+} by cations having a larger ionic ratio than Ca^{2+}, such as Sr^{2+}, preferentially occurs in the orthorhombic lattice of aragonite, whereas cations having a smaller ionic ratio than Ca^{2+}, such as Mg^{2+}, are more readily incorporated in the hexagonal lattice of calcite (Speer, 1983; Huang and Fairchild, 2001; Finch and Allison, 2007; Day and Henderson, 2013). Consequently, the Sr concentration, and thus the Sr/Ca ratio are sensitive to mineralogy.

Recently, Scroxton et al. (2018) used Sr concentrations measured by Core-Scanning micro X-ray Fluorescence (CS-μXRF) as a reliable approximate of Sr/Ca because the near constant Ca concentration orders of magnitude higher than Sr in calcite and aragonite implies that the sole Sr variability controls variability of Sr/Ca. In the P-XRF analyses of the Pont-de-Ratz speleothems, variability of Sr concentration at fine spatial scale in either primary aragonite or primary calcite is not detectable, and variability of Sr concentration faithfully reflects proportions of aragonite and calcite mineralogies.

6.1.2. Strontium as a tool for identifying areas affected by recrystallization

In the Pont-de-Ratz speleothems, the two types of secondary calcite yielded very different Sr concentrations (Table 3). The values of Sr in secondary sparry calcites are intermediate between those of aragonite and those of primary columnar calcite (Fig. 5A). This is explained by the presence of abundant relicts of the aragonite precursor in the secondary sparry crystals (Perrin et al. 2014, their Fig. 12 p. 260) (Fig. 7C). Similarly, high Sr-values have been reported in inclusion-rich part of secondary calcite from the Wadi Sannur speleothems, with Sr values comparable to Sr concentration of spelean aragonites and much higher than primary spelean calcites (Railsback et al., 2002). These results clearly show that using P-XRF for a first geochemical screening of the speleothem slabs is an efficient tool for detecting areas initially in aragonite and partly or entirely recrystallized into sparry calcite.

By contrast, primary and secondary columnar calcites yielded overlapping Sr values (Fig. 5A; Table 3). In the Pont-de-Ratz speleothems, aragonite relicts are much rarer in secondary columnar calcite than in secondary sparry calcite (Perrin et al., 2014). Due to their scarcity, aragonite relicts occurring in secondary columnar calcite are not detected by the P-XRF spectrometer and thus both columnar calcites show similar Sr values.

In the Pont-de-Ratz speleothems, the Sr content of secondary calcite thus dominantly relies on the recrystallization process. Aragonite-to-calcite recrystallization is known to drastically modify the initial Sr/Ca, and at the same time Mg/Ca (e.g., Dominguez-Villar et al., 2017; Scroxton et al., 2018) preventing their use as environmental proxies. In the Pont-de-Ratz cave, the extent of this modification depends on the type of recrystallization process and more specifically on the recharge rate of the diagenetic fluid with respect to the recrystallization kinetics as this trade-off directly controls the amount of aragonite relics preserved in the secondary calcite crystals (Perrin et al., 2014) (Table 2).

6.1.3. P-XRF as a tool for detecting detrital input

Among the other recorded elements, only Fe and Mn reach significant values (Table 3, Supplementary data file). Except for the Fe-rich stalagmite PDR22, the distribution of both Fe and Mn in the Pont-de-Ratz speleothems is patchy and irregular at the sample scale. Their presence is related to small amounts of detrital and non-authigenic material such as clays, occurring in speleothem pores and/or interstices between carbonate crystals. P-XRF is therefore also an efficient technique for rapidly detecting detrital inputs entrapped in speleothems. This is particularly useful for climatic studies since such detrital material can impact both the precision of radiometric dating and the stable isotope signature.

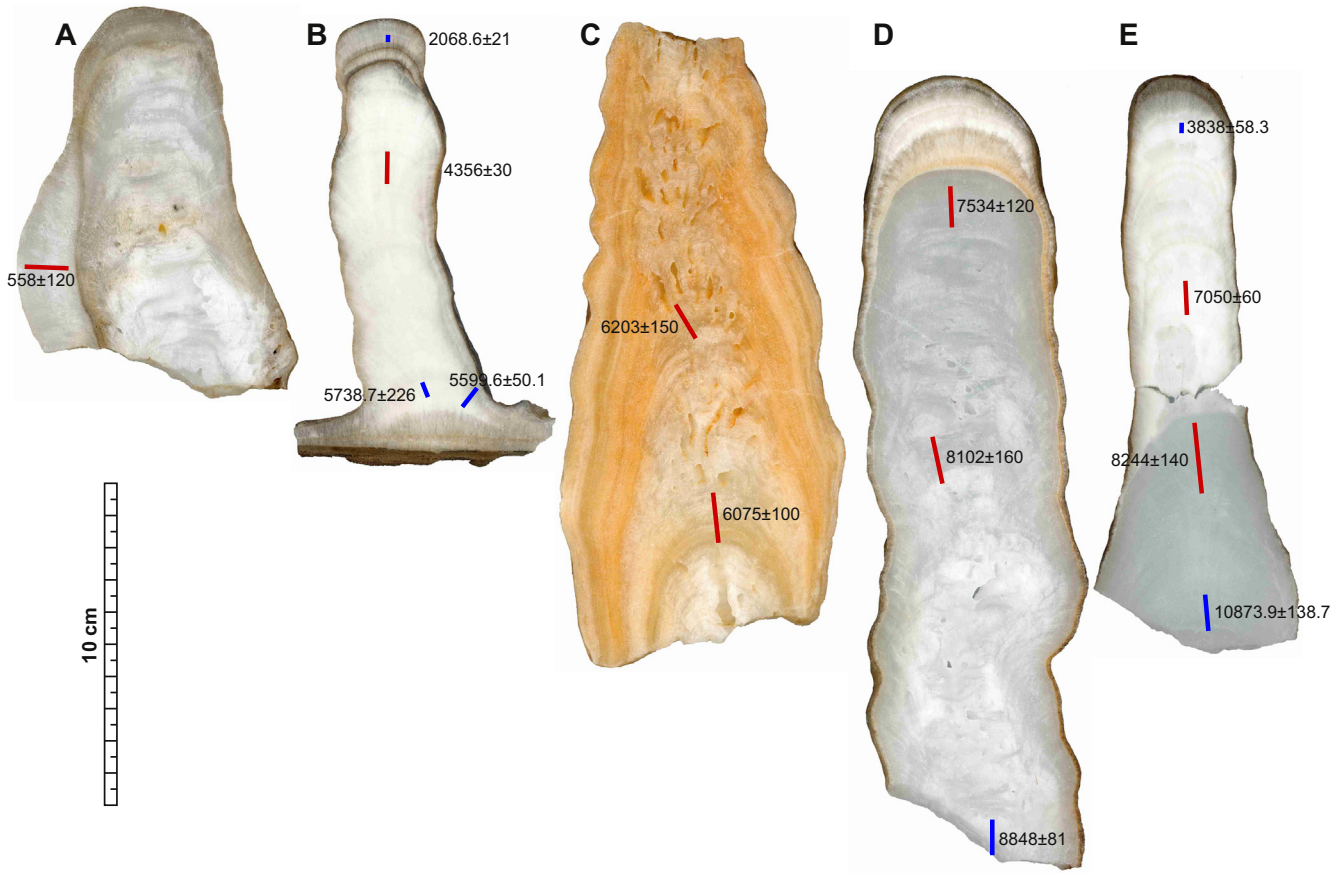

Fig. 9. U/Th dating results shown on stalagmite slabs. Bars represent the thickness of the U/Th subsamples with respect to lamination. Red bars correspond to TIMS U/Th analyses, and blue bars to MC-ICP-MS U/Th analyses. Age values are given in years. (A) Slab of stalagmite PDR3. (B) Slab of stalagmite PDR17. (C) Slab of stalagmite PDR22. (D) Slab of stalagmite PDR20. (E) Slab of stalagmite PDR21. (For interpretation of the references to color in this figure legend, the reader is referred to the web version of this article.)

6.2. Petrographical maps

Mapping the growth discontinuities and the primary and secondary carbonate products from petrographical and mineralogical study of thin section provides a synthetic document having the spatial resolution of a thin section at low-to-medium magnification and the coverage of most, if not all, surface of the speleothem slab (Fig. 6D). These petrographical maps: (1) clearly report the distributional patterns of the identified petrographical features; (2) allow the preserved and altered areas to be precisely and rapidly visualized at the scale of individual speleothem; and (3) precisely show the succession of growth units and growth discontinuities. In the Pont-de-Ratz speleothems, the petrographical maps revealed an efficient guide for selecting the position of subsamples for U/Th dating in primary carbonates.

Several works have reported the value of alternating aragonite-calcite layers as recorder of wet-dry conditions (e.g., Railsback et al., 1994; McMillan et al., 2005). It is likely that the alternating calcite and aragonite growth units of the Pont-de-Ratz speleothems recorded such a paleoclimatic signal. Beyond the goal of optimizing subsampling, these petrographical maps offer the possibility to anchor the successive aragonite and calcite growth phases in a reliable chronological framework and, therefore, to establish the growth history of the Pont-de-Ratz speleothems and explore their paleoclimate and paleoenvironmental significance.

6.3. Speleothem U-series dating

Aragonite and calcite subsamples from stalagmites of the Pont-de-Ratz cave have narrow ranges for U concentrations although these ranges show strong differences between both polymorphs. U concentrations are much higher (more than 45 times higher) in primary aragonite than in primary columnar calcite (Table 4, Fig. 8). Such differences have been already reported in speleothem carbonates by several authors (e.g., Railsback et al., 2002; Dominguez-Villar et al., 2017; Frisia et al., 2018) and result from fractionation for U in aragonite being much larger than in calcite (Kitano and Oomori, 1971; Meere and Benninger, 1993). As reported in various studies, calcites resulting from recrystallization of aragonite generally yield high U concentrations as a consequence of the presence of aragonite relicts trapped in the secondary calcite (e.g., Railsback et al., 2002; Pickering et al., 2010; Lachniet et al., 2012a; Dominguez-Villar et al., 2017). Therefore, a set of values from both primary and secondary calcites displays a much wider range of U concentration than a group of values from primary calcites only (Railsback et al., 2002). In the Pont-de-Ratz dataset, the narrow ranges of U concentration in primary aragonites and primary calcites respectively, confirm the non-altered nature of these subsamples and thus the reliability of our approach.

Although a particular case of aragonite-to-calcite recrystallization, in which U and Th evolve as a semi-closed system and are inherited by the secondary calcite, was described by Dominguez-Villar et al. (2017), most aragonite-to-calcite recrystallizations occur in open-system conditions for U and Th and alters radiometric dating by yielding anomalously older ages (Richards and Dorale, 2003; Hoffman et al., 2009; Lachniet et al., 2012a; Scholz et al., 2014). Such ages can be easily misinterpreted if the secondary nature of calcite is not recognized through a prior petrographic assessment of speleothem diagenesis.

Another common cause of reversals in U/Th ages is the introduction of detrital thorium in the spelean material to be dated, either initially at the primary precipitation stage, or afterwards during subsequent

speleothem growth stages. When high detrital $^{230}Th/^{232}Th$ ratios are suspected, a correction is applied, although it has been demonstrated that in some cases this correction is not sufficient (Hellstrom, 2006; Fensterer et al., 2010; Hoffmann et al., 2010; Scholz et al., 2012) and leads to older age estimates (Lachniet et al., 2012a).

In our Pont-de-Ratz speleothem samples, the ^{232}Th concentrations do not show marked disparities between primary aragonite and primary calcite and no correction was necessary (Table 4).

The final results of U/Th dating of five stalagmites from the Pont-de-Ratz cave show ages in good chronological order in individual stalagmites and coherent between them (Fig. 9). Aragonite speleothems can be used for paleoenvironmental, dating and/or paleoclimatic purposes given that their diagenetic state is carefully evaluated and understood. On the other hand, in calcite speleothems, calcite cannot be considered as a priori primary, in particular when cave conditions, such as dolomitic host rocks, may have been favorable to aragonite formation. Understanding the diagenetic pathways undergone by the initial spelean material and careful mapping, at an appropriate scale, the primary and diagenetic products on stalagmite slabs, revealed a particularly effective way to precisely select where subsamples for U/Th dating and paleoclimate studies should be taken.

7. Conclusions and perspectives

Built on multiscale petrographical and geochemical data obtained from a combination of analytical techniques, our integrated approach offers a reliable way to determine with precision the position of subsamples for further investigation, such as radiometric dating or proxy analysis. This research provides the main following results:

- P-XRF is an easy-to-use, rapid and non-destructive in-situ technique, which can directly be applied on polished speleothem slabs for initial geochemical screening.
- Trace-element content obtained from P-XRF was used in three different ways for optimizing subsampling. Since Sr content is correlated with carbonate mineralogy, Sr values can thus be used to infer the spatial distribution of areas formed by aragonite or by calcite. Intermediate values of Sr are indicators of areas initially in aragonite and partly or entirely recrystallized into sparry calcite. Fe and Mn content reflect the distribution of detrital deposits in the speleothem and, hence, can be used as a warning about potential detrital contamination prior to subsampling for U/Th dating.
- As they allow the preserved and altered areas to be precisely vizualized at the scale of the speleothem slab, petrographical maps are an efficient tool for selecting the position of subsamples for U/Th dating.
- U geochemistry is also correlated with mineralogy. The respective narrow ranges of U concentration in primary columnar calcites on one hand, and primary aragonites on the other, corroborate the primary nature of these precipitates and the excellent state of preservation of the U—Th dating subsamples.
- The remarkable coherence of U/Th results both within and between the five individual stalagmites of the Pont-de-Ratz cave is a convincing example of the reliability of our approach and shows that petrography constitutes the most reliable tool for evaluating speleothem preservation prior to more specific investigations.
- The Pont-de-Ratz speleothems record several alternating growth phases of aragonite and calcite precipitation, with potential paleoclimate significance. Although samples are partly impacted by diagenesis, the proposed methodological approach and the large set of speleothem samples should allow this interesting archive to be unlocked.

Acknowledgments

Access to the cave was facilitated by the two speleological clubs of the Saint-Ponais and the city of Saint-Pons-de-Thomières. Technical preparation of samples and thin-sectioning is particularly acknowledged: Michel Lemoine, Lilian Case, Vincent Rommevaux (MNHN), Jean-François Mena (University of Toulouse). Valuable assistance was provided by Gilles Montagnac (ENS Lyon) with Raman microspectrometry. The company Aquila-Conseil nicely provided the P-XRF spectrometer. Uranium dating analyses were performed by Bassam Ghaleb (Geotop, MacGill University, Montréal, Canada). We specially thank Patrick Cabrol (DREAL Midi-Pyrénées, France) for assistance in the field and numerous fruitful discussions at different steps of this research. Andrea Columbu, an anonymous reviewer and Jasper Knight, Editor of Sedimentary Geology are sincerely thanked for their helpful and constructive comments.

Appendix A. Supplementary data

Results of the P-XRF analyses from the speleothems of the Cimetière chamber in Pont-de-Ratz cave. Supplementary data to this article can be found online at https://doi.org/10.1016/j.sedgeo.2019.06.002.

References

Alabouvette, B., Demange, M., De Sauval, C., Autrelle, C., 1993. Notice explicative, Carte géol. France (1/50 000), feuille Saint-Pons (1013). BRGM, Orléans 123 pp.
Bajo, P., Hellstrom, J., Frisia, S., Drysdale, R., Black, J., Woodhead, J., Borsato, A., Zanchetta, G., Wallace, M.W., Regattieri, E., Haese, R., 2016. "Cryptic" diagenesis and its implications for speleothem geochronologies. Quat. Sci. Rev. 148, 17–28.
Cabrol, P., 1978. Contribution à l'étude du concrétionnement carbonaté des grottes du Sud de la France, morphologie, genèse, diagenèse. Mémoires du Centre d'Etudes et de Recherches Géologiques et Hydrogéologiques 12, Montpellier.
Cabrol, P., Coudray, J., 1982. Climatic fluctuations influence the genesis and diagenesis of carbonate speleothems in southwestern France. National Speleological Society Bulletin 44, 112–117.
Columbu, A., Drysdale, R., Capron, E., Woodhead, J., De Waele, J., Sanna, L., Hellstrom, J., Bajo, L., 2017. Early last glacial intra-interstadial climate variability recorded in a Sardinian speleothem. Quat. Sci. Rev. 169, 391–397.
Day, C.C., Henderson, G.M., 2013. Controls on trace-element partitioning in cave-analogue calcite. Geochim. Cosmochim. Acta 120, 612–627.
Dominguez-Villar, D., Krklec, K., Pelicon, P., Fairchild, I.J., Cheng, H., Edwards, L.R., 2017. Geochemistry of speleothems affected by aragonite to calcite recrystallization – potential inheritance from the precursor mineral. Geochim. Cosmochim. Acta 200, 310–329.
Fensterer, C., Scholz, D., Hoffmann, D.L., Mangini, A., Pajon, J.M., 2010. $^{230}Th/U$ dating of a late Holocene low uranium speleothem from Cuba. IOP Conference Series: Earth and Environment Science 9, 012015 https://doi.org/10.1088/1755-1315/9/1/012015.
Finch, A.A., Allison, N., 2007. Coordination of Sr and Mg in calcite and aragonite. Mineral. Mag. 71, 539–571.
Finch, A.A., Shaw, P.A., Weedon, G.P., Holmgren, K., 2001. Trace element variation in speleothem aragonite: potential for palaeoenvironmental reconstruction. Earth Planet. Sci. Lett. 186, 255–267.
Finch, A.A., Shaw, P.A., Holmgren, K., Lee-Thorp, J., 2003. Corroborated rainfall records from aragonitic stalagmites. Earth Planet. Sci. Lett. 215, 265–273.
Frisia, S., Borsato, A., Fairchild, I.J., McDermott, F., Selmo, E.M., 2002. Aragonite - calcite relationships in speleothems (Grotte de Clamouse, France): environment, fabrics, and carbonate geochemistry. J. Sediment. Res. 72, 687–699.
Frisia, S., Borsato, A., Hellstrom, J., 2018. High spatial resolution investigation of nucleation, growth and early diagenesis in speleothems as exemplar for sedimentary carbonates. Earth-Sci. Rev. 178, 68–91.
Gázquez, F., Calaforra, J.M., Forti, P., Stoll, H., Ghaleb, B., Delgado-Huertas, A., 2014. Paleoflood events recorded by speleothems in caves. Earth Surf. Process. Landf. 39, 1345–1353.
Genty, D., Combourieu-Nebout, N., Peyron, O., Blamart, D., Wainer, K., Mansuri, F., Ghaleb, B., Isabello, L., Dormoy, I., von Grafenstein, U., Bonelli, S., Landais, A., Brauer, A., 2010. Isotopic characterization of rapid climatic events during OIS3 and OIS4 in Villars Cave stalagmites (SW-France) and correlation with Atlantic and Mediterranean pollen records. Quat. Sci. Rev. 29, 2799–2820.
Hellstrom, J.C., 2006. U/Th dating of speleothem with high initial ^{230}Th using stratigraphical constraint. Quat. Geochronol. 1, 289–295.
Hercman, H., Pawlak, J., 2012. MOD-AGE: an age-depth model construction algorithm. Quat. Geochronol. 12, 1–10.
Hoffman, D.L., Spötl, C., Mangini, A., 2009. Micromill and in situ laser ablation sampling techniques for high spatial resolution MC-ICPMS U/Th dating of carbonates. Chem. Geol. 259, 253–261.
Hoffmann, D.L., Beck, J.W., Richards, D.A., Smart, P.L., Singarayer, J.S., Ketchmark, T., Hawkesworth, C.J., 2010. Towards radiocarbon calibration beyond 28 ka using speleothems from the Bahamas. Earth Planet. Sci. Lett. 289, 1–10.
Hopley, P.J., Marshall, J.D., Latham, A.G., 2009. Speleothem preservation and diagenesis in South African Hominin sites; implications for paleoenvironments and geochronology. Geoarchaeology 24, 519–547.
Huang, Y., Fairchild, I.J., 2001. Partitioning of Sr^{2+} and Mg^{2+} into calcite under karst-analogue experimental conditions. Geochim. Cosmochim. Acta 65, 47–62.

Kitano, Y., Oomori, T., 1971. The coprecipitation of uranium with calcium carbonate. J. Oceanogr. Soc. Jpn 27, 34–43.
Lachniet, M.S., 2015. Are aragonite stalagmites reliable paleoclimate proxies? Tests for oxygen isotope time-series replication and equilibrium. GSA Bull. 127, 1521–1533.
Lachniet, M.S., Bernal, J.P., Asmerom, Y., Polyak, V., 2012a. Uranium loss and aragonite – calcite age discordance in a calcitized aragonite stalagmite. Quat. Geochronol. 14, 26–37.
Lachniet, M.S., Bernal, J.P., Asmerom, Y., Polyak, V., Piperno, D., 2012b. A 2400 yr Mesoamerican rainfall reconstruction links climate and cultural change. Geology 40, 259–262.
Lazar, B., Enmar, R., Schossberger, M., Bar-Matthews, M., Halicz, L., Stein, M., 2014. Diagenetic effects on the distribution of uranium in live and Holocene corals from the Gulf of Aqaba. Geochim. Cosmochim. Acta 68, 4583–4593.
Li, R., Jones, B., 2013. Temporal and spatial variations in the diagenetic fabrics and stable isotopes of Pleistocene corals from the Ironshore Formation of Grand Cayman, British West Indies. Sediment. Geol. 286, 58–72.
Martin-Garcia, R., Alonzo-Zarza, A.M., Martin-Pérez, A., 2009. Loss of primary texture and geochemical signatures in speleothems due to diagenesis: evidences from Castañar Cave, Spain. Sediment. Geol. 221, 141–149.
Martin-Garcia, R., Alonzo-Zarza, A.M., Frisia, S., Rodriguez-Berriguete, A., Drysdale, R., Hellstrom, J., 2019. Effect of aragonite to calcite transformation on the geochemistry and dating accuracy of speleothems. An example from Castañar Cave, Spain. Sediment. Geol. 383, 41–54.
McMillan, E.A., Fairchild, I.J., Frisia, S., Borsato, A., McDermott, F., 2005. Annual trace element cycles in calcite-aragonite speleothems: evidence of drought in the western Mediterranean 1200–1100 yr BP. J. Quat. Sci. 20, 423–433.
Meere, D.E., Benninger, L.K., 1993. The coprecipitation of Pu and other radionuclides with $CaCO_3$. Geochim. Cosmochim. Acta 57, 1447–1458.
Perrin, C., Smith, D.C., 2007a. Decay of organic skeletal matrices as control on early diagenesis of coral skeletons. C R Palevol 6, 253–260.
Perrin, C., Smith, D.C., 2007b. Earliest steps of diagenesis in living coral skeletons: evidence from ultrastructural pattern and Raman spectroscopy. J. Sediment. Res. 77, 495–507.
Perrin, C., Prestimonaco, L., Servelle, G., Tilhac, R., Maury, M., Cabrol, P., 2013. Growth and diagenetic history of aragonite-calcite speleothems, implications for environmental studies. In: Filippi, M., Bosak, P. (Eds.), Proceedings 16th International Congress of Speleology 2. 21–28 July 2013, Brno, Czech Republic, pp. 447–449.
Perrin, C., Prestimonaco, L., Servelle, G., Tilhac, R., Maury, M., Cabrol, P., 2014. Aragonite-calcite speleothems: identifying original and diagenetic features. J. Sediment. Res. 84, 245–269.
Pickering, R., Kramers, J.D., Partridge, T., Kodolanyi, J., Pettke, T., 2010. U-Pb dating of calcite-aragonite layers in speleothems from hominin sites in South Africa by MC-ICP-MS. Quat. Geochronol. 5, 544–558.
Pozzi, J.-P., Rousseau, L., Falguères, C., Mahieux, G., Deschamps, P., Shao, Q., Kachi, D., Bahain, J.-J., Tozzi, C., 2019. U-Th dated speleothem recorded geomagnetic excursions in the Lower Brunhes. Sci. Rep. 9, 1114. https://doi.org/10.1038/s41598-018-38350-4.
Railsback, L.B., Brook, G.A., Chen, J., Kalin, R., Fleisher, C.J., 1994. Environmental controls on the petrology of a late Holocene speleothem from Botswana with annual layers of aragonite and calcite. J. Sediment. Res. A64, 147–155.
Railsback, L.B., Dabous, A.A., Osmond, J.K., Fleisher, C.J., 2002. Petrographic and geochemical screening of speleothems for U-series dating: an example from recrystallized speleothems from Wadi Sannur Cavern, Egypt. Journal of Cave and Karst Studies 64, 108–116.
Ribaud-Laurenti, A., Hamelin, B., Montaggioni, L., Cardinal, D., 2001. Diagenesis and its impact on Sr/Ca ratio in Holocene Acropora corals. International Journal of Earth Science 90, 438–451.
Richards, D., Dorale, J., 2003. Uranium-series chronology and environmental applications of speleothems. Rev. Mineral. 52, 407–460.
Scholz, D., Hoffmann, D.L., 2011. StalAge – an algorithm designed for construction of speleothem age models. Quat. Geochronol. 6, 369–382.
Scholz, D., Hoffmann, D.L., Hellstrom, J., Ramsey, C.B., 2012. A comparison of different methods for speleothem age modelling. Quat. Geochronol. 14, 94–104.
Scholz, D., Tolzmann, J., Hoffmann, D.L., Jochum, K.P., Spötl, C., Riechelmann, D.F.C., 2014. Diagenesis of speleothems and its effect on the accuracy of ^{230}Th/U-ages. Chem. Geol. 387, 74–86.
Scroxton, N., Burns, S., Dawson, P., Rhodes, J.M., Brent, K., McGee, D., Heijnis, H., Gadd, P., Hantoro, W., Gagan, M., 2018. Rapid measurement of strontium in speleothems using core-scanning micro X-ray fluorescence. Chem. Geol. 487, 12–22.
Speer, J.A., 1983. Crystal chemistry and phase relations of orthorhombic carbonates. Rev. Mineral. Geochem. 11, 145–190.
Woo, K.S., Choi, D.W., 2006. Calcitization of aragonite speleothems in limestone caves in Korea: diagenetic process in a semiclosed system. In: Harmon, R.S., Wicks, C. (Eds.), Perspectives on Karst Geomorphology, Hydrology, and Geochemistry: A Tribute Volume to Derek C. Ford and William B. White. Geological Society of American Special Paper 404, Boulder, CO, pp. 297–306.
Zhang, H., Cai, Y., Tan, L., Qin, S., An, Z., 2014. Stable isotope composition alteration produced by the aragonite-to-calcite transformation in speleothems and implications for paleoclimate reconstructions. Sediment. Geol. 309, 1–14.